

A DETECTION OF THE COLD IMPRINT OF VOIDS ON THE MICROWAVE BACKGROUND RADIATION

YAN-CHUAN CAI¹, MARK C. NEYRINCK², ISTVÁN SZAPUDI³, SHAUN COLE¹ AND CARLOS S. FRENK¹

¹Institute for Computational Cosmology, Department of Physics, University of Durham, South Road, Durham DH1 3LE, UK

²Department of Physics and Astronomy, The Johns Hopkins University, 3701 San Martin Drive, Baltimore, MD 21218, USA

³Institute for Astronomy, University of Hawaii, 2680 Woodlawn Drive, Honolulu HI 96822, USA

Draft version March 10, 2019

ABSTRACT

We measure the average cold spot on the cosmic microwave background (CMB) produced by voids selected in the SDSS DR7 spectroscopic redshift galaxy catalog, spanning redshifts from 0 to 0.4. Our detection has a significance of $\sim 3\sigma$ based on the variance of random samples, and has an average amplitude of $\sim 3\mu\text{K}$ as viewed through a compensated top-hat filter scaled to the radius of each void. This signal, if interpreted as the late-time Integrated Sachs-Wolfe effect, serves as an evidence for the late-time acceleration of the Universe. The detection is achieved by applying the optimal filter size identified from N -body simulations. Two striking features are found by comparing ISW simulations with our detection, 1.) the void profiles traced by halos in our simulations are very similar to those in the data traced by galaxies. 2.) the same filter radius that gives the largest ISW signal in simulations also yields the largest detected signal in the observations. We model the expected ISW signal using voids from N -body simulations in ΛCDM , selected in the same way as in the observations. The detected signal, however, is many times larger than that from simulations, discrepant at the $\sim 3\sigma$ level. The large cosmic variance of large-scale modes in the gravitational potential can obscure an ISW measurement such as ours. However, we show how this cosmic variance can be effectively reduced by using a compensated top-hat filter for the detection. We test whether a few possible systematic effects could be producing the signal; we find no evidence that they do.

Subject headings: cosmic microwave background — cosmology: observations — large-scale structure of universe — methods: statistical

1. INTRODUCTION

The late-time Integrated Sachs-Wolfe effect (ISW) (Sachs & Wolfe 1967) is direct evidence of cosmic acceleration (Crittenden & Turok 1996). However, detection of the ISW effect by the cross-correlation of large-scale structure and the cosmic microwave background (CMB) is challenging, due to large cosmic variance and possible systematics. Combined analysis of a few different galaxy/QSO surveys has yielded a signal of estimated significance $\sim 4\sigma$ (Giannantonio et al. 2008; Ho et al. 2008; Giannantonio et al. 2012), although there are alternative views (e.g., Sawangwit et al. 2010). These, and most other, analyses have used a cross-correlation-function method, which captures the ISW signal if both the galaxy density field and the ISW signal are Gaussian.

Another method exploits the physical insight that in the presence of dark energy, linear-scale voids and superclusters stretch faster than they can grow through gravity. Voids should produce ISW cold spots, and superclusters hot spots. Granett et al. (2008, G08) stacked 100 such quasilinear-scale structures, reporting a detection of corresponding cold and hot spots at $4\text{-}\sigma$ significance. The non-linear ISW, the Rees-Sciama (RS) effect (Rees & Sciama 1968) may come to confuse the stacked signal, but it is expected at low redshift only at the $\sim 10\%$ level at $z < 1$ on sub-degree scales (Cai et al. 2009, 2010). The significance level of the detection from this single galaxy sample seems to be higher than the cross-correlation method, while the amplitude of the signal is found to be 2 to 3σ higher than estimates from simulations, indicating tension with the concordance cosmology at $z \sim 0.5$ where the sig-

nal is from (G08 Nadathur et al. 2012; Pápai & Szapudi 2010; Pápai et al. 2011). Incorporating the contribution of non-linearity seems unable to reduce this tension (Flender et al. 2012; Hernandez-Monteagudo & Smith 2012). It is therefore important to check if such a signal/tension persists in other epochs of the Universe, and in other void catalogs.

In this paper, we re-investigate this issue using a new, independent SDSS void catalog (Sutter et al. 2012) which uses essentially the same void-finder as G08 used, with a few differences in selection criteria. Compared to the previous sample, which used photometric redshifts, the current sample uses galaxies both with accurate spectroscopic redshifts, and, at low redshift, much higher sampling, allowing more accurate knowledge of each void's physical structure. The current sample covers the redshift range $0 < z < 0.44$, complementary to the previous catalog, which spans $0.4 < z < 0.75$.

In section 2 of our paper, we briefly describe the void catalog, and details of stacking. Section 3 presents simulations of the void catalog and the ISW signal. Main results are presented in section 4. We summarize tests for systematics in section 5 and draw conclusions in section 6.

2. VOID CATALOG

We use the void catalog presented by Sutter et al. (2012). Voids are identified in both the SDSS DR7 main-galaxy sample and the luminous-red-galaxy (LRG) samples. The main sample covers 8500 deg^2 on the sky. It has a redshift range of $0 < z < 0.2$ and the LRG sample is at $0.16 < z < 0.44$. Six volume-limited samples are made

out of these two samples. They are *dim1* ($0 < z < 0.05$), *dim2* ($0.05 < z < 0.1$), *bright1* ($0.1 < z < 0.15$), *bright2* ($0.15 < z < 0.2$), *lrgdim* ($0.16 < z < 0.36$) and *lrgbright* ($0.36 < z < 0.44$). The number density of galaxies decreases with redshift. The parameter-free ZOBOV (Neyrinck 2008) algorithm was applied to find voids from those galaxy samples, with some modifications to give more-explicit hierarchical information (Lavaux & Wandelt 2012). ZOBOV tessellates space into Voronoi cells around each galaxy, and applies a watershed algorithm (e.g. Platen et al. 2007) on the irregular Delaunay mesh to group those cells into zones.

Whereas G08 used a cut of about 3σ in statistical significance (compared to voids in a Poisson process) to get the 50 voids and 50 clusters in their analysis, the selection criteria in the present void catalog are quite different. The Poisson-process significance level was most appropriate in the previous photometric sample, where the key was simply to detect voids or clusters at all, but more-physical criteria may be applied to the present sample. We use the criteria used by Sutter et al. (2012), which were not designed specifically for ISW detection, but they still give a void catalog suitable for it. First, when deciding whether to merge possibly spuriously separate neighboring voids with a given void, a threshold of $\delta \leq -0.8$ is applied to neighboring voids. Second, voids are eliminated with overdensities $\delta > -0.8$, as estimated in a sphere of radius $(1/4)r_v$ about the volume-weighted void center, where r_v is the effective void radius, $[3/(4\pi)V]^{1/3}$. Third, voids with r_v smaller than the mean galaxy separation are eliminated. Void centers are defined to be the volume-weighted average of all member galaxies. Survey boundaries and the mask are accounted for by removing voids that intersects a boundary galaxy when rotating in any direction about their centers. We restrict our analysis to this ‘central sample’ that is less affected by boundaries. The total number of voids in this sample is 776.

Going from low to high redshift, the galaxy sampling decreases, giving larger-physical-radius voids (see Fig. 7 and 8 of Sutter et al. (2012)). Higher sampling allows more structure to be seen, i.e. smaller voids and sub voids to be detected. The majority of voids in the catalog have radii of $r_v \sim 10 - 20$ Mpc/h and they are found in a relatively small volume within $z < 0.15$, while the highest-redshift sub-sample at $z \sim 0.4$ has voids with $r_v > 70$ Mpc/h.

3. SIMULATIONS

For testing our analysis pipeline and to understand the expected ISW signal, we construct mock void catalogs from N -body simulations and compute their expected ISW signal from a Λ CDM universe. Our goal is to perform the same analysis in the SDSS data as in our simulated voids where the ISW signal is known.

3.1. Simulations of voids

We construct mock void catalogs using a set of simulations run in the concordance cosmology ($\Omega_m = 0.24, \Omega_\Lambda = 0.76, n_s = 0.958, \sigma_8 = 0.77, h = 0.73$) (Li et al. 2013). The simulations are run with three different box sizes and number of particles [$L=1500$ Mpc/h, $N_p=1024^3$], [$L=1000$ Mpc/h, $N_p=1024^3$] and [$L=250$

Mpc/h, $N_p=512^3$]. We use halos matched to the number densities of galaxies in the 6 volume limited sub-samples of the SDSS data. Halos with more than 20 particles linked by the Friends-of-Friends algorithm with the linking length of 0.2 (Davis et al. 1985). The particle mass of our simulations are $2.09 \times 10^{11} M_\odot/h$, $6.20 \times 10^{10} M_\odot/h$ and $0.77 \times 10^{10} M_\odot/h$, therefore the minimal halo masses in the catalog are $M_{\min} \sim 4.18 \times 10^{12} M_\odot/h$, $1.24 \times 10^{12} M_\odot/h$ and $1.54 \times 10^{11} M_\odot/h$. Halos are approximated as galaxies, assuming that each main halo hosts one SDSS galaxy. This simple treatment neglects the complexity of galaxy formation and halo occupation. In the densest galaxy samples, for example, large halos should host multiple galaxies, better delineating void edges. Excluding these extra galaxies may reduce our ability to detect voids in the simulations. But given that we rely on halos just to find voids, and the typical sizes of voids are usually orders of magnitude larger than the size of halos, the simulated void catalog should be acceptable for our purposes.

To model the signal, it is important to match the galaxy sampling density, since more, and smaller, structures are found with increasing sampling. We adjust M_{\min} to match the number density of galaxies in those volume limited samples except for the two lowest-redshift sub-samples, where the number density of galaxies are beyond the resolution limit of our current simulations. In principle, we can use a higher-resolution simulation to match these densities. But given that the volume of these two sub-samples are less than 2% of the total, we expect them to contribute very little to the final stacked signal, which will be demonstrated in the next section. We therefore do not make the effort to analyze higher resolution simulations, and leave it for future work. The two highest redshift sub-samples from LRGs has the largest average voids and occupy the largest volume among the six sub-samples. To reduce cosmic variance, we employ 6 realizations of the simulation with $L = 1500$ Mpc/h.

We apply the same void finding algorithm as in the real data to these mock halo catalogs and find voids at 4 discrete redshift slices, $a = 0.7, 0.8, 0.9, 1.0$ in the cubic simulation boxes, where a is the expansion factor. This covers the whole redshift range of the SDSS void catalog.

3.2. Simulations of ISW

For each simulation box, we follow the algorithm presented by Cai et al. (2010) to compute the time derivative of the potential $\dot{\Phi}$ using particle data. This can be achieved by computing $\dot{\Phi}$ in Fourier space using

$$\dot{\Phi}(\vec{k}, t) = \frac{3}{2} \left(\frac{H_0}{k} \right)^2 \Omega_m \left[\frac{\dot{a}}{a^2} \delta(\vec{k}, t) + \frac{i\vec{k} \cdot \vec{p}(\vec{k}, t)}{a} \right], \quad (1)$$

where a is the expansion factor, $\vec{p}(\vec{k}, t)$ is the Fourier transform of the momentum density divided by the mean mass density, $\vec{p}(\vec{x}, t) = [1 + \delta(\vec{x}, t)]\vec{v}(\vec{x}, t)$, and $\delta(\vec{k}, t)$ is the Fourier transform of the density contrast. H_0 and Ω_m are the present values of the Hubble and matter density parameters. The inverse Fourier transform of the above yields $\dot{\Phi}$ in real space on 3D grids. The integration of $\dot{\Phi}$ along the line-of-sight yields the full linear and nonlinear

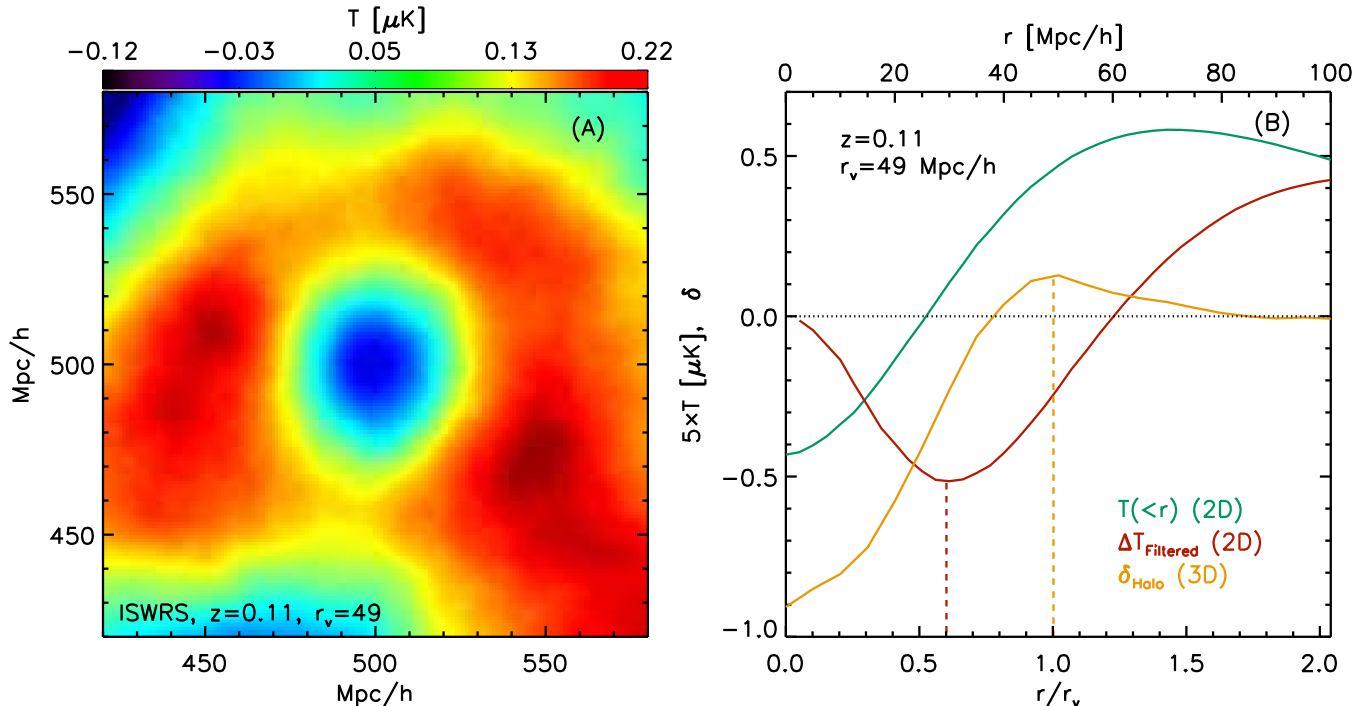


FIG. 1.— From N -body simulations, the stacked ISWRS 2D temperature (A) and the 1D average cumulative temperature profile (green-solid on panel-B) for simulated voids with radius $r_v \approx 49$ Mpc/h. In panel-A, 3D void density profiles traced by halos are shown in orange. The red-solid line is obtained from convolving the average 2D projected ISW temperature map with compensated top-hat filters of different radii R . The red-dash line indicates the filter radius where the ISW temperature reaches its minimum (maximum in absolute value). It is about 60% of the effective void radius traced by halo number density, as indicated by the orange-dash line. The zero-crossing of the green curve is very close to the radius where the filtered ISW signal peaks. These profiles come from the stacking of 475 voids within the radius of 45 to 55 Mpc/h identified using halos at $a = 0.9$ from the simulation with the box size of $L=1000$ Mpc/h. For the ISWRS maps, Fourier modes with $k < 0.01h/\text{Mpc}$ are removed to reduce the noise. The temperatures on the B panel are multiplied by a factor of 5 for better illustration.

ISW temperature fluctuation (ISWRS),

$$\Delta T(\hat{n}) = \frac{2}{c^2} \int \dot{\Phi}(\hat{n}, t) dt. \quad (2)$$

In the linear regime, the velocity field is related to the density field by the linearized continuity equation $\vec{p}(\vec{k}, t) = i\dot{\delta}(k, t)\vec{k}/k^2 \approx i\beta(t)\delta(k, t)\vec{k}/k^2$. Thus

$$\dot{\Phi}(\vec{k}, t) = \frac{3}{2} \left(\frac{H_0}{k} \right)^2 \Omega_m \frac{\dot{a}}{a^2} \delta(\vec{k}, t) [1 - \beta(t)], \quad (3)$$

where $\beta(t)$ denotes the linear growth rate $\beta(t) \equiv d \ln D(t) / d \ln a$. This equation is the conventional way of modeling the ISW effect and uses only the information from the density field. Integrations of the above equation along the line-of-sight gives a set of 2D ISW temperature maps for different redshifts.

4. STACKING OF VOIDS

4.1. Stacking in simulations

With the simulated void catalogs and the simulated ISWRS and ISW maps, we can do the same stacking as in the observations, and make predictions of the expected ISW signal in the concordance cosmology.

We follow a similar procedure as G08 for stacking superstructures, with the key difference being that we scale the filter radius to each void. In G08, a constant filter radius was used because photometric redshift errors prevented accurate estimates of physically meaningful void

radii. In contrast, the current sample allows more accurate estimates.

The filtered CMB signal around each void is the temperature averaged over a circular aperture $r < R$ around the void center, minus the temperature averaged over a surrounding annular aperture $R < r < \sqrt{2}R$:

$$\Delta T = \bar{T}_1 - \bar{T}_2 = \frac{\int_0^R T(\vec{r}) d\vec{r}}{\int_0^R d\vec{r}} - \frac{\int_R^{\sqrt{2}R} T(\vec{r}) d\vec{r}}{\int_R^{\sqrt{2}R} d\vec{r}}, \quad (4)$$

where R is the radius of the filter. We use ΔT for filter temperature and reserve T for the unfiltered temperature throughout the paper. The main purpose of this filter is to suppress large-scale power contamination from the primordial CMB. In reality, void profiles are not compensated top-hats, and this filter is likely not the optimal for ISW detection. However, as long as we perform the same convolution for both the real data and simulations, direct comparisons between them are fair and meaningful. This relatively simple convolution enables us to adjust the size of the filter according to the size of each void with ease; the optimal ratio of the filter size R and the ZOBOV void size is determined from simulations.

With this aim, simulated voids of similar radii at the same redshifts are stacked. This is done for both the halo number density field and the 3D ISW signal, i.e. $\dot{\Phi}$ on 3D grids. Then, the stacked 3D grids of $\dot{\Phi}$ are projected along all three axes of the cubic simulation box to reduce cosmic variance for the measured ISW signal.

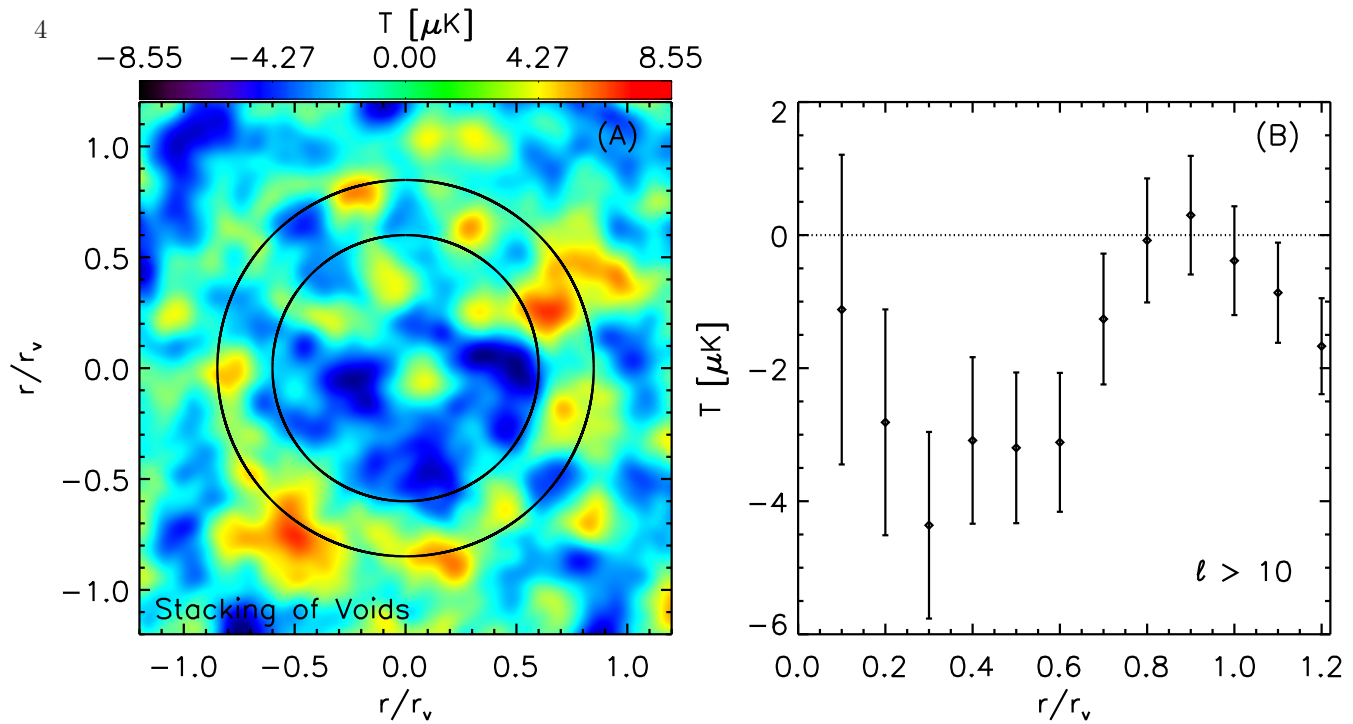


FIG. 2.— Stacking of WMAP9 V-band maps using all the 776 voids from the SDSS DR7 galaxy sample. A – the 2D image of the stacked map. It is smoothed by a Gaussian filter with $\text{FWHM}=0.08r_v/r$. Before stacking, each map has been rescaled by the void radius so that they all match in the unit of r/r_v as shown in the x and y axes. The radii of the inner and outer circles are 0.6 and $0.6\sqrt{2}$ of the effective radii of the compensated top-hat filter. B – the 1D averaged profile of the stacked map. Modes with $\ell \leq 10$ have been removed from the CMB map to reduce the influence of large-scale temperature perturbations.

This yields the 2D stacked ISW temperature ΔT map, as shown on Fig. 1-A. A cold spot corresponding to the stack of 475 voids is clearly seen, as expected. The map is then convolved with compensated top-hat filters of different radii, from which filtered ISW temperatures corresponding to the void region are found.

Here we see that quasilinear or nonlinear-scale voids generally have overdense shells around them. Indeed, that is roughly the definition of a ZOBOV void. The ISW signals of these nonlinear voids generally have hot rings around them, as shown in the green curve of Fig. 2. So, although it has been argued that an uncompensated filter is of equal value in detecting features in the CMB (Zhang & Huterer 2010), at least for detection of an ISW-like void or supercluster imprint, use of a compensated filter is justified, and greatly preferred.

To find the optimal filter radius for a given void effective radius, we explore a wide range of filter radii in our simulations. The Fig. 1-B shows the filtered ISW temperature versus filter radius R for voids of the average radius $r_v \sim 49 \text{ Mpc}/h$ (red line). We also plot the cumulative ISW temperature profile without convolution with the filter in green and the 3D halo density profile in orange. Interestingly, we find that the filtered ISW signal peaks at $R \sim 0.6r_v$, i.e. at significantly smaller values than the measured void radius, roughly coinciding with the zero-crossing of the ISW temperature profile. The optimal filter size appears to be independent of redshift, and it is weak function of the void radius, it increases to approximately 0.7 for $r_v > 70 \text{ Mpc}/h$. We implement this nearly universal filter size as a “rescaling factor” before stacking for the analysis of the SDSS data.

Compared to the density field, the potential (and its time derivative) carries an extra factor of $1/k^2$, causing

scales much larger than the voids in the catalog to dominate the ISW temperature maps. To reduce this large-scale variance, we remove some very large-scale modes ($k < 0.01h/\text{Mpc}$) when showing the ISW temperature map and profiles. Even with the k -mode removal and the stacking of 475 voids, the ISW cold spot still does not seem very spherical. The influence of cosmic variance is still strong. Perhaps for the same reason, we have also found that with k -mode removal at different scales, the 2D cold spot and the cumulative ISW temperature profile (green line) may change significantly, while the red curve (filtered ISW temperature versus filter radius) is relatively stable, as long as removed k -modes are much larger than the size of voids. This suggests that the 2D compensated top-hat filter indeed helps reduce the influence of large-scale perturbation modes. Lending credence to our mocks, the halo number-density profiles look similar to the galaxy density profiles from the SDSS data shown in Fig. 9 of Sutter et al. (2012) for a wide range of void radius.

4.2. Stacking with SDSS data

In individual voids, the expected ISW signal we are interested in is overwhelmed by two major sources of noise, 1.) the primordial CMB temperature fluctuations, 2.) the ISW temperature fluctuations that have larger coherent scales than the typical size of our voids. These noise sources, which are essentially cosmic variance, are much greater than the ISW signal for which we are looking. It is therefore necessary to suppress them so that we can detect the ISW signal with the available stack. For this purpose, we use two techniques. First, we remove large-scale modes from the CMB, i.e. $\ell \leq 10$, knowing that these scales are much larger than the sizes of our

voids and the sought ISW signal will not be affected by the removal of them. All results we show in the rest of the paper have the $\ell \leq 10$ restriction unless specified otherwise. Second, we apply compensated top-hat filters to the CMB, hoping to further reduce the influence of large-scale modes. Of course, stacking a large number of voids can also help to reduce the noise. Detailed tests on the influence of cosmic variance will be addressed in the next subsection.

We use the WMAP9 foreground-reduced Q, V and W frequency maps (Bennett et al. 2012) for the stack, excluding voids which overlap by $> 20\%$ with WMAP masked regions. This reduces the number of voids slightly, from 776 to 761.

Before stacking, each CMB map has been rescaled by the void radius. Fig. 2-A shows the 2D stacking of WMAP9 V-band maps to 1.2 times the rescaled radius around the common void center. An extended cold region at the center of the figure surrounded by a hot ring is clearly seen, with the coldest pixel of $\sim -8.5\mu\text{K}$ when smoothed by a Gaussian filter of $\text{FWHM}=0.08 r_v/r$. The corresponding 1D profile is shown in Fig. 2-B. Except for a slight up turn close to the center, all data points are consistently negative within 0.9 of the rescaled radius. This is in qualitative agreement with (Granett et al. 2008), where the stack of 50 voids also yields a cold spot surrounded by a hot ring. We will elaborate our discussion of this point in the next subsection.

Now we apply compensated filters to our maps. As in the simulated maps, the filter size for each void is 60% of its radius. Filtered CMB temperatures are sorted by void radius and stacked. The solid lines on the top panel of Fig. 3 shows the cumulative stacked CMB temperature ΔT versus the number of stacks, using the WMAP9 Q, V and W-band maps. Except for a fluctuation on the noisy, low-void-number end, the stacked CMB temperature is negative, an indication of the stability of the signal. The stacked temperature varies from $-2.3\mu\text{K}$ to $-6.0\mu\text{K}$, and the variation decreases with the number in the stack, as expected. It reaches -2.8 , -2.9 and $-3.0\mu\text{K}$ for Q, V and W bands, respectively, when all SDSS voids are used for the stacking. This suggests no frequency dependence. We repeat the same stacking with the CMB monopole and dipole removed, and find -2.6 , -2.7 and $-2.9\mu\text{K}$ for Q, V and W bands. This changes are negligibly small.

To estimate the statistical significance, we measure the noise in two ways. First, we hold the sizes of all voids fixed but randomize their positions on the sky when stacking. The WMAP mask is applied in the same way as we do for the original stacking. We estimate the variance of the stacked temperatures from 5000 such randomizations. The resulting curve of the variances is shown as dotted line in Fig. 3. Second, we use the best-fit CMB power spectrum (Larson et al. 2011) to generate 5000 mock CMB maps, and repeat the same stacking with them. The variances of the random sample are nearly the same as those from the first method, at the percent level. This indicates the robustness of noise estimation.

The signal-to-noise ratio (S/N) of the stacking is shown in the bottom panel of Fig. 3. With a certain amount of fluctuation, the S/N is in general increasing with the number of voids in the stacks. By ~ 200 , it reaches 3σ . The stacking of all SDSS voids yields $\sim 3\sigma$.

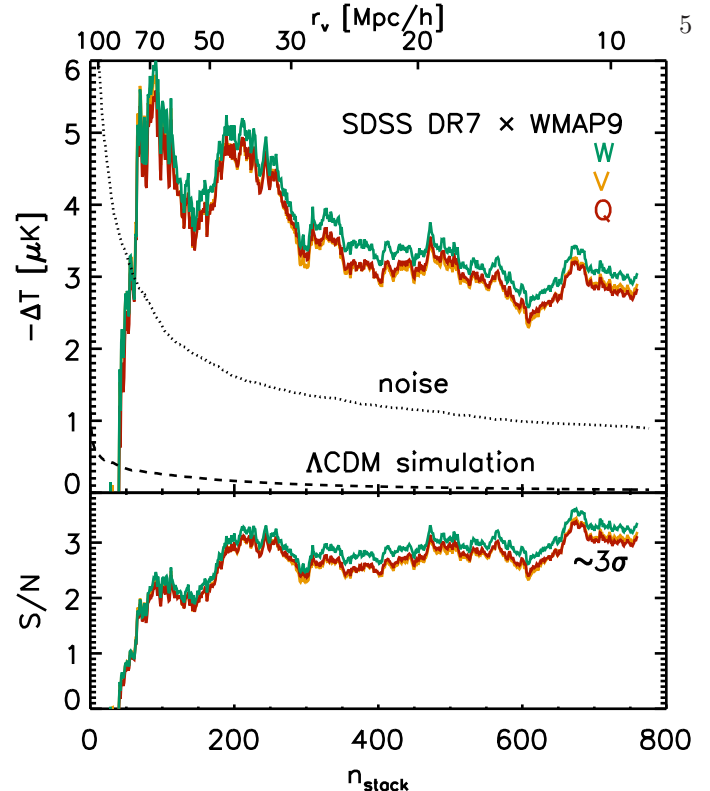


FIG. 3.— Stacking of WMAP9 Q (red), V (orange), W (green)-band maps using void catalogs from the SDSS DR7 galaxy sample. In the upper panel, the solid curve shows the cumulative stacks of the compensated-filtered CMB temperature. Voids are sorted by size, which increases from the left to the right. The black-dotted line is the variance calculated from randomizing the sky position of each void 1000 times and repeat the stacking. The dashed line is the stacked linear+nonlinear ISW signal in the fiducial concordance cosmology using simulated void catalogs described in section 3. The lower panel shows the cumulative signal-to-noise ratio (S/N) for each stack. After stacking about 200 voids, we get a $\sim 3\sigma$ detection.

Qualitatively, this negative temperature fluctuation corresponding to the stacking of voids is expected from the linear ISW effect in the ΛCDM Universe. Therefore, this signal may be an evidence that the expansion of the Universe at $0 < z < 0.44$ is accelerating. However, quantitative cosmological interpretation of the signal is complicated by the two factors. First, even without cosmic acceleration, the CMB temperature fluctuation induced by a void via the Rees-Sciama effect is also negative (Cai et al. 2010). This nonlinear ISW effect may be important at relatively small scales, especially for the majority of the SDSS voids with the radius of 10 to 20 Mpc/h . Secondly, accurate modeling of the ISW signal for a void is difficult without the precise knowledge of the void profile, and the profile is certainly stochastic. Our simulations presented in section 3 provide a perfect way to remove these two obstacles.

4.3. Cosmic variance

Before comparing our detection with simulations, we want to address the most dominant source of noise in this measurement, cosmic variance. It consists of two components, the primordial CMB temperature fluctuations and the ISW temperature fluctuations that have larger coherent scales than our typical void sizes. The importance of the second noise source is due to the proportionality $\Phi \propto 1/k^2$ that makes the power spectrum

of $\dot{\Phi}$ rise very steeply with the decreasing of k . These two sources of noise can be at least a few times, and up to orders of magnitude greater than the ISW signal for which we are looking.

Suppose in an optimistic case, the expected ISW signal is of the order of $1 \mu\text{K}$ for voids of $r_v \sim 100 \text{ Mpc}/h$, as shown in Fig. 5 and the CMB temperature fluctuation are of the order of $30 \mu\text{K}$. Assuming the noise in the stack goes down as $1/\sqrt{N}$, one will need a stack of 8100 voids to make a 3σ detection. This is far beyond the reach of any existing data. As another example, if we have voids with the radii of $r_v \sim 50 \text{ Mpc}/h$ at $z \sim 0.1$ as shown in Fig. 1, given the $1\text{Gpc}/h$ simulation boxsize, the projected 2D ISW temperature fluctuations are of the order of a $10 \mu\text{K}$, while the ISW temperature from the void is at the order of $0.1 \mu\text{K}$. To reach a 3σ detection in this case, even without the primordial CMB fluctuations, the number of voids we would need to stack is ~ 90000 .

To demonstrate further the significant influence of cosmic variance and the effectiveness of our filtering techniques to reduce it, we try retaining in the CMB maps only perturbation modes with $\ell > 0, 1, 2, 5, 10, 20, 30$ and 40 , and repeat our analysis. Results are shown in Fig. 4. The following interesting results are found:

(1) When removing low- ℓ modes of the WMAP map from $\ell_{\min} \sim 1$ to 30 , the amplitude of the stacked CMB temperature profile of voids may change as much as $10\mu\text{K}$, including changing from positive to negative, but the overall shape of the stacked profile is preserved (Fig. 4-A). However, the top-hat-compensated-filtered stacked temperature is almost not affected by the low- ℓ mode removal. It only changes by a few percent within the range of ℓ_{\min} that we have explored (Fig. 4-B). Moreover, the errorbars on the profile decrease with increasing ℓ_{\min} , as expected. The importance of cosmic variance is evident. Clearly, the stacked CMB temperature of voids is affected by large-scale temperature perturbations whose scales are much greater than the typical scale of voids. Without any filtering, the number of stacks we have is not enough to beat down the large-scale perturbations. The compensated filter reduces the influence of large-scale modes, greatly stabilizing our signal.

(2) In Fig.4-A, the profile become stable within the mode removal range of about $10 < \ell_{\min} < 30$. This is also expected. With a small ℓ_{\min} (< 10), the remaining influence of cosmic variance may still be large, while with a large ℓ_{\min} (> 30), part of the ISW signal may be affected by the mode removal, which is not what we want. Given that the majority of our voids have radii of 2 to 4 degrees, the corresponding ISW signal contributed from them should not be much larger than this typical scale. Such an ISW signal should not be affected by eliminating modes with only $\ell \leq 10$. This is why we choose to show our results using CMB maps with $\ell > 10$ in this paper.

(3) While the amplitude of the stacked profile is not expected to be stable with $\ell_{\min} < 10$, when removing only the CMB monopole and dipole, i.e. the case of

$\ell > 1$ shown in orange in the Fig. 4-A, the amplitude of the profile turns out to be nearly the same as the case of $\ell > 10$. The stacking of all 761 voids in the SDSS survey sky happens to have done the same job as to eliminate the influence of those modes with $1 < \ell \leq 10$. Note however, the amplitudes of the stacked profiles do not usually appear to be the same as $\ell > 10$ for other cases such as $l > 0, 2$ and 5 . We have noticed that in G08, stacking only 50 voids over a similar patch of the sky also yields a cold spot, with only the monopole and dipole removed from the CMB. This coincidence is somewhat surprising given that the number of voids in their stack is much smaller than ours.

(4) In Fig. 2, there is an obvious temperature dip within the void radius. As expected, we see a 2D cold spot, surrounded by a hot ring, as shown in Fig. 1. However, the innermost temperature point is a bit surprisingly high in Fig. 2. Given the rather large error bars, this may be simply noise. On the other hand, we have seen similar things in our simulations of voids (with the same selection criteria as in the data). When the void radius is smaller than about twice of the mean halo (galaxy) separation, the simulated stacked ISW temperature also turns slightly upward. This may be related to ZOBOV's definition of a void as a density depression around a local-density-minimum galaxy, using the Voronoi tessellation. That means that if, in the CMB stack, we were to define void centers as local-density-minimum galaxies, there would always be a density peak (a galaxy) at the center, not desirable. We largely eliminate this problem by instead defining the center as the volume centroid (usually not at the position of a galaxy), but perhaps the influence of a central, least-dense galaxy in the void persists at some level, pushing this innermost point upward. Arguably, using the dual, Delaunay tessellation, in which the cells are not around each galaxy, but are the spaces between galaxies, could be better for void-finding. Likely, there is room for improvement in the void-finding algorithm, or selection criteria, for ISW detection. But we did not wish to tinker with these issues in this paper, to avoid *a posteriori* bias.

4.4. Comparison with simulations

We compare our measurement with simulations in this subsection. With the simulations presented in Section 3, we can compute the mean filtered ISWRS temperature ΔT for voids of different sizes at different redshifts. Essentially, we will have a table of $\Delta T(r_v, z)$ from a large number of samples. We simply take the mean filtered temperature and neglect stochasticity of the void profiles because cosmic variance is usually dominant over stochasticity for $\Delta T(r_v, z)$. In total, we have 13120 voids in the volume of $21.26 (\text{Gpc}/h)^3$ in our simulations, which is more than 10 times that of the SDSS data. The resulting curves of $\Delta T(r_v)$ are shown in Fig. 5. The size and redshift dependence of the ISWRS temperature is clearly seen, i.e. larger voids induce a greater ISWRS signal, and, show the increasing influence of dark energy. A void at constant r_v has larger $|\Delta T|$ at larger scale factor. Voids with $r_v < 20 \text{ Mpc}/h$ have $|\Delta T| < 0.1\mu\text{K}$ at

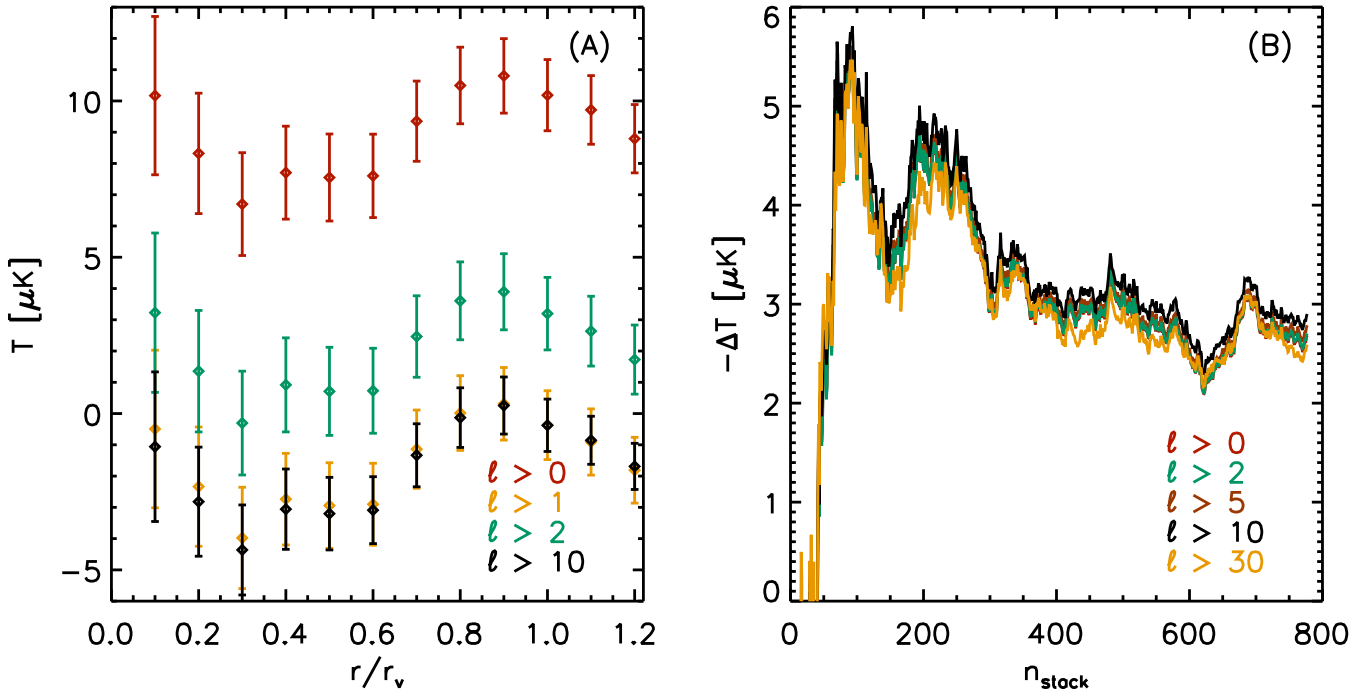


FIG. 4.— A— the same as the Fig. 2-B but showing results with different minimal mode cut off ℓ_{\min} for the CMB as labelled in the figure. B— the cumulative stacks of the compensated-filtered CMB temperature, like the top panel of Fig. 3 but with different ℓ_{\min} . 1.) in panel A, the overall amplitude of the profile shifts up and down by a large amount for different values of ℓ_{\min} , while the compensated-filtered temperature remains stable as shown in panel B, with only a few percents variation with different ℓ_{\min} s shown in the plot. 2.) The errorbars in the A panel decrease as ℓ_{\min} increases 3.) In the A panel, the profile becomes stable within the mode removal range of about $10 < \ell_{\min} < 30$.

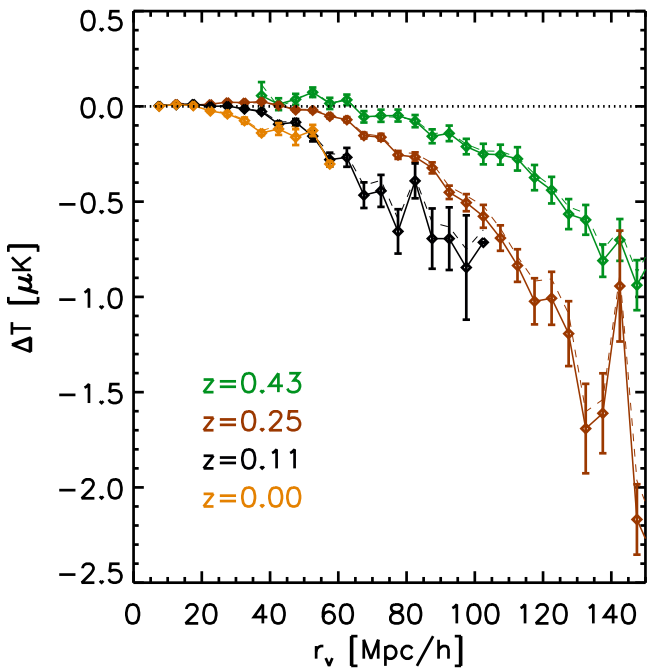


FIG. 5.— Filtered ISW+RS temperature for voids of different radii at different redshifts from simulations, measured as in the observations. Dashed lines indicate the linear ISW signal. We linearly interpolate from these curves to compute the simulated stacking signal of the ISW+RS from the SDSS DR7 void catalog.

all redshifts. The largest voids found in the SDSS data ($r_v \sim 140 \text{ Mpc}/h$) may have $|\Delta T| \sim 1 - 2 \mu\text{K}$, but they are very rare. The magnitude of the linear ISW signal is typically 10% to 20% lower than the full ISWRS signal. Larger differences are found for smaller voids such as $r_v < 20 \text{ Mpc}/h$, but the overall amplitudes there are negligibly small.

We sample from the table of $\Delta T(r_v, z)$ for the 761 voids with the same sizes and redshifts as in the SDSS data, and obtain the simulated curve of cumulative stacked ΔT versus the number of voids in the stack for this cosmology, as shown by the dashed line in Fig. 3. The magnitude of the simulated ISWRS signal is substantially smaller than the observed one. If there is no other contamination or systematics, the data suggest a $2-3\sigma$ tension with the ΛCDM cosmology.

5. POTENTIAL SYSTEMATICS

In principle, stacking CMB temperature maps using voids should suffer little contamination from other astrophysical processes, in that voids are relatively empty. The frequency independence of the result shown in the previous section suggests that it is unlikely to come from contamination by radio sources or the thermal SZ effect (Sunyaev & Zeldovich 1972). It is also unlikely to be contaminated by the kSZ effect, which arises from the line-of-sight bulk motion of free electrons relative to the CMB. For the kSZ effect to induce the observed temperature decrement in voids, a void would have to have a high column density of free electrons. The center of the void would have to be moving away from us, but

not the overdense ring around it, an unlikely set of circumstances. Nevertheless, we do the following tests to investigate other potential systematics:

(1) We try varying the rescaling factor for the size of the filter radius and find the resulting stacked temperature is indeed close to the maximum when using the 0.6 factor indicated by the simulations. Results are shown in Fig. 6. Intriguingly, the same scaling factor of 0.6 that gives the largest amplitudes of the filtered ISW temperature also gives the largest signal in the data. This consistency with simulations regarding the optimal filter size is encouraging. It also seems to suggest that our detected signal may have very similar profile as the simulated ISW signal (when comparing Fig. 6 to the red curve of Fig. 1-B).

(2) To test if there is any Galactic contamination, we plot the filtered temperatures versus Galactic coordinates of the voids in Fig. 4. We find that at relatively low Galactic latitude, $b < 30$ ($b = 0$ being the Galactic plane), the average filtered temperature is positive. This might indicate some unknown contamination in the CMB from near the Galaxy, but the statistics are very poor. It may well be just random noise. There is no clear dependence of the signal on Galactic longitude.

(3) To test the dependence of the signal on the void size, we plot the filtered temperature versus the effective void radius in Fig. 4. We find the signal has no strong dependence on the void radius. This might seem to contradict what we have found from simulations, that large voids are expected to have larger filtered temperature, but again the statistics are too poor to tell.

(4) To test if the signal is dominated by any individual volume-limited sample, we find the stacked CMB temperature using each of the sub-samples separately. We find that all six individual stacks yield negative filtered temperatures: $-2.2\mu\text{K}$, $-2.4\mu\text{K}$, $-2.6\mu\text{K}$, $-4.7\mu\text{K}$, $-3.0\mu\text{K}$ and $-4.6\mu\text{K}$ from low- z to high- z samples. This is expected if there are no systematic errors.

Finally, we have noticed the slight up turn of the stacked temperature profile towards the center of the stacked region, and have suspected that it is likely due the noise in the void catalog or noise of the CMB. In principle, we can use our simulation to purify our sample by removing some voids with small radii. However, this may introduce *a posteriori* bias. We therefore do not trim down our the sample on this basis. For the same reason, we do not want to restrict ourselves to using only part of the sample, e.g. individual volume-limited samples.

6. CONCLUSIONS AND DISCUSSION

We have found that the stacking CMB temperatures around the positions of voids from the SDSS DR7 spectroscopic galaxy catalog yields a temperature decrement of $\sim 3\mu\text{K}$, a detection with about $3\text{-}\sigma$ significance. To avoid *a posteriori* bias, we use all the 776 voids in the catalog without applying any further restriction on the data. When interpreted as the ISW or Rees-Sciama effect, it is at odds with simulations of a ΛCDM universe at $\sim 3\sigma$.

We use simulations of voids and the ISW effect to understand our detection. We have found the void profiles are very similar in the simulations as in the data, and that the same optimal filter radius that gives the largest

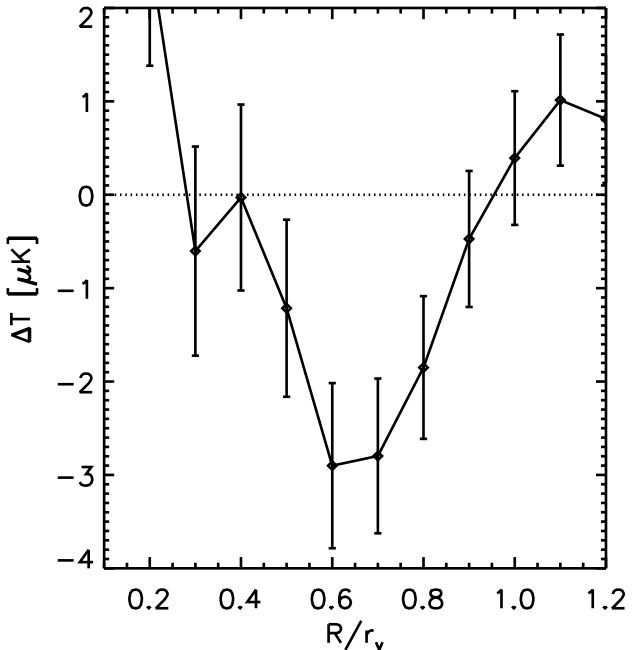


FIG. 6.— The observed, stacked void signal (in Fig. 2-A, unsmoothed), viewed through compensated top-hat filters of different radii R/r_v . It is to be compared with the red curve in Fig. 1-B.

ISW signal also yields the largest detection in the data. These similarities between simulations and observation, though qualitative, may suggest the robustness of our detection.

We have also demonstrated that the detection of the ISW signal is strongly influenced by large-scale perturbation modes, which is essentially cosmic variance. Applying compensated top-hat filters can effectively reduce such an influence from both the primordial CMB and the ISW effect on large scales.

Our findings bolster the results of Granett et al. (2008, G08), and vice-verse. The detected signals both go the same way, a much larger magnitude than expected in a ΛCDM universe. The G08 statistical significance was 4.4σ including both voids and clusters, and 3.7σ including only the voids. The present result is not entirely independent from G08, since they both use the CMB in the SDSS footprint, and there is a tiny overlap in redshift; this sample spans $z = 0\text{-}0.44$, while the G08 sample spans $z = 0.4\text{-}0.75$. The consistency of the two results is striking, and intriguing. Additionally, the support our results provide to the G08 detection, in which supervoids and superclusters were detected in a photometric-redshift galaxy sample, suggests that photometric redshifts may suffice for the detection of these large structures.

In principle, the tension between the detection of the ISW signal with the ΛCDM model could be resolved by invoking non-Gaussianity. However the value of f_{NL} needed may be at the order of ~ 1000 (Hernandez-Monteagudo & Smith 2012), which is inconsistent with constraints from the CMB (e.g. Komatsu et al. 2011). Alternatively, voids in some models of modified gravity may grow larger and faster than in the ΛCDM universe, giving a larger ISWRS signal (Clampitt et al. 2012). Whether or not such models can

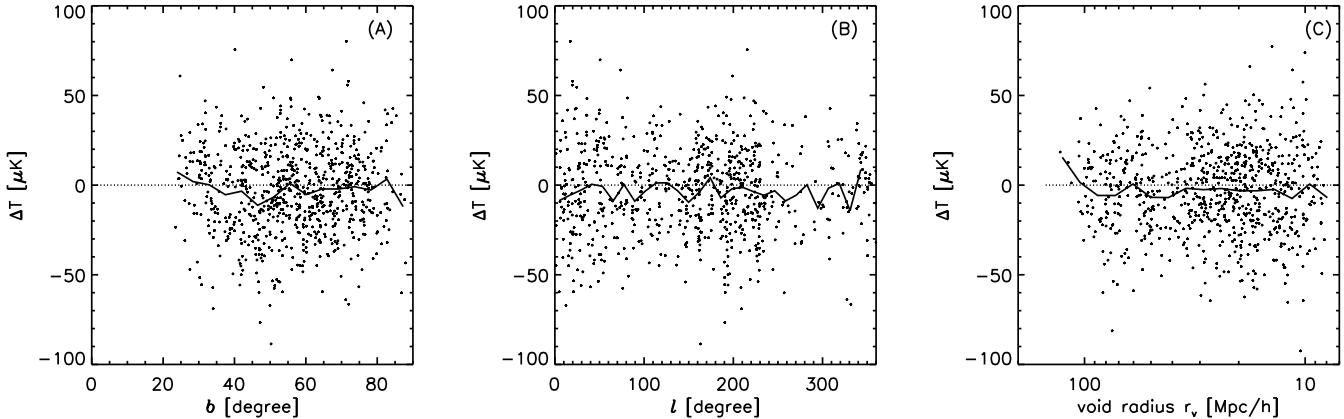


FIG. 7.— Filtered CMB temperature versus X , X =Galactic latitude (A), Galactic longitude (B) or void radius r_v (C), sorted by different quantities as indicated. In Galactic coordinate system, $l = 0$ is the Galactic plane.

tolerate the high amplitude of the ISW signal while not violating other observational constraints of cosmology remains an open question. Further investigation of this issue with surveys of larger volume and sky coverage is also needed to firmly confirm/resolve this tension.

ACKNOWLEDGMENTS

We thank P. M. Sutter for making public the SDSS DR7 void catalog and for his helpful discussions and comments on the manuscript. We thank Baojiu Li for providing the N -body simulations. MN is grateful for support from a New Frontiers grant from the Sir John Templeton Foundation. YC is supported by the Durham Junior Research Fellowship.

REFERENCES

- Bennett, C. L., Larson, D., Weiland, J. L., et al. 2012, ArXiv e-prints, arXiv:1212.5225
- Cai, Y.-C., Cole, S., Jenkins, A., & Frenk, C. 2009, MNRAS, 396, 772, 772
- Cai, Y.-C., Cole, S., Jenkins, A., & Frenk, C. S. 2010, MNRAS, 407, 201, 201
- Clampitt, J., Cai, Y.-C., & Li, B. 2012, ArXiv e-prints, arXiv:1212.2216
- Crittenden, R. G., & Turok, N. 1996, Physical Review Letters, 76, 575, 575
- Davis, M., Efstathiou, G., Frenk, C. S., & White, S. D. M. 1985, ApJ, 292, 371, 371
- Flender, S., Hotchkiss, S., & Nadathur, S. 2012, ArXiv e-prints, arXiv:1212.0776
- Giannantonio, T., Crittenden, R., Nichol, R., & Ross, A. J. 2012, MNRAS, 426, 2581, 2581
- Giannantonio, T., Scranton, R., Crittenden, R. G., et al. 2008, Phys. Rev. D, 77, 123520, 123520
- Granett, B. R., Neyrinck, M. C., & Szapudi, I. 2008, ApJ, 683, L99, L99
- Hernandez-Montegudo, C., & Smith, R. E. 2012, MNRAS, submitted, arXiv:1212.1174
- Ho, S., Hirata, C., Padmanabhan, N., Seljak, U., & Bahcall, N. 2008, Phys. Rev. D, 78, 043519, 043519
- Komatsu, E., Smith, K. M., Dunkley, J., et al. 2011, ApJS, 192, 18, 18
- Larson, D., Dunkley, J., Hinshaw, G., et al. 2011, ApJS, 192, 16, 16
- Lavaux, G., & Wandelt, B. D. 2012, ApJ, 754, 109, 109
- Li, B., Hellwing, W. A., Koyama, K., et al. 2013, MNRAS, 428, 743, 743
- Nadathur, S., Hotchkiss, S., & Sarkar, S. 2012, JCAP, 6, 42, 42
- Neyrinck, M. C. 2008, MNRAS, 386, 2101, 2101
- Pápai, P., & Szapudi, I. 2010, ApJ, 725, 2078, 2078
- Pápai, P., Szapudi, I., & Granett, B. R. 2011, ApJ, 732, 27, 27
- Platen, E., van de Weygaert, R., & Jones, B. J. T. 2007, MNRAS, 380, 551, 551
- Rees, M. J., & Sciama, D. W. 1968, Nature, 217, 511, 511
- Sachs, R. K., & Wolfe, A. M. 1967, ApJ, 147, 73, 73
- Sawangwit, U., Shanks, T., Cannon, R. D., et al. 2010, MNRAS, 402, 2228, 2228
- Sunyaev, R. A., & Zeldovich, Y. B. 1972, Comments on Astrophysics and Space Physics, 4, 173, 173
- Sutter, P. M., Lavaux, G., Wandelt, B. D., & Weinberg, D. H. 2012, ApJ, 761, 44, 44
- Zhang, R., & Huterer, D. 2010, Astroparticle Physics, 33, 69, 69